Molecular Therapy
Methods & Clinical Development
Original Article

Silencing hepatic PCSK9 via novel chimeric AAV8 mitigates the progression of atherosclerosis by inhibiting inflammation in ApoE$^{-/-}$ mice

Xiaocui Chen,[1,2] Minghui Sun,[4] Xiang Ma,[1,3] Yitong Ma,[1,3] and Bangdang Chen[1,2]

[1]Xinjiang Key Laboratory of Cardiovascular Disease Research, State Key Laboratory of Pathogenesis, Prevention and Treatment of High Incidence Diseases in Central Asia, Clinical Medical Research Institute, First Affiliated Hospital of Xinjiang Medical University, Urumqi 830054, P.R. China; [2]Basic Medical College, Xinjiang Medical University, Urumqi 830011, P.R. China; [3]Department of Cardiology, First Affiliated Hospital of Xinjiang Medical University, Urumqi 830054, P.R. China; [4]Department of Nephrology, Fifth Affiliated Hospital of Xinjiang Medical University, Urumqi 830000, P.R. China

Adeno-associated virus (AAV) is the most widely utilized vector for gene therapy. Proprotein convertase subtilisin/kexin type 9 (PCSK9), predominantly expressed in the liver, plays a crucial role in lipid regulation and atherosclerosis progression. Here, we developed a novel chimeric AAV8.P-PCSK9 short hairpin RNA (shRNA) vector that incorporates a cross-species specific shRNA targeting PCSK9 to assess its effects on lipid levels and atherosclerosis in mice. AAV8.P demonstrated superior transduction efficiency and safety, achieving about 90% liver transduction and maintaining transgene expression for up to a year. The AAV8.P-PCSK9 shRNA exhibited typical liver-tropism and effectively silenced hepatic PCSK9. Moreover, it significantly lowered serum cholesterol and triglyceride levels while increasing LDL-R level without causing hepatotoxicity in wild-type mice. Additionally, it decreased PCSK9 expression and elevated low-density lipoprotein receptor expression in Apolipoprotein E-deficient mice, leading to early changes in lipid profiles but lacking a sustained impact on circulating lipids. Importantly, silencing PCSK9 resulted in reduced plaque areas with enhanced stability, decreased inflammatory macrophage infiltration, and lower levels of vascular and systemic inflammatory markers. These findings indicate that targeted silencing of hepatic PCSK9 significantly reduces lipid levels and effectively mitigates atherosclerosis progression by inhibiting inflammatory responses via the AAV8.P-PCSK9 shRNA vector, thereby providing critical support for its clinical translation.

INTRODUCTION

Atherosclerosis is the primary pathology underlying cardiovascular diseases (CVDs),[1] the leading cause of morbidity and mortality worldwide.[2] Atherosclerosis is characterized by lipid deposition and chronic inflammation within the vascular system.[3–5] Statins are the most effective treatment, targeting low-density lipoprotein-cholesterol (LDL-C) to prevent and treat the condition. However, a relatively large percentage of high-risk patients with CVD, who are statin intolerant/resistant, fail to achieve ideal LDL-C levels despite undergoing intensive statin therapy. Proprotein convertase subtilisin/kexin type 9 (PCSK9) is mainly synthesized in the liver.[6] It binds to the low-density lipoprotein receptor (LDL-R) and promotes its degradation, resulting in increased circulating LDL-C levels.[7,8] PCSK9 has become an important target for drug discovery and development of prevention and treatment strategies against atherosclerotic cardiovascular disease (ASCVD).[9,10]

Innovative PCSK9 inhibitory therapies, including three monoclonal antibodies (mAbs) (evolocumab, alirocumab, and tafolecimab) and one small interfering RNA (siRNA) (inclisiran) represent a significant breakthrough in CVD. PCSK9 mAbs showed great efficacy in reducing plasma LDL-C levels and the risk of ASCVD events, but the clinical application of mAbs is costly and requires regular and long-term administration due to the short in vivo half-life of the mAbs.[11] Inclisiran, an siRNA that inhibits PCSK9 synthesis, is a newly approved drug for patients with hypercholesterolemia or mixed dyslipidemia.[12] It provides potential benefits such as a reduced risk of major cardiovascular events.[13] Compared with mAb drugs, inclisiran provides longer-lasting effects,[14,15] but the agent has not been widely used due to its high cost and clinical application requirements.[16] Other alternative approaches to inhibit PCSK9, such as vaccines and gene editing strategies, are being actively developed and undergoing clinical evaluation.[17–19]

The ongoing clinical success of AAV gene therapy against hemophilia has heightened the enthusiasm for developing AAV gene therapies against liver diseases due to the natural hepatic tropism of the vector.[20,21] A key attractive feature of AAV8 is represented by the high levels of hepatocyte gene transfer and the long-term liver transduction achieved after a peripheral vein injection of the vector.[22] The activity of the secretory phospholipase A2 protein (sPLA2) associated with the capsid protein is critical for the infectivity of viral vectors

Received 6 May 2024; accepted 3 December 2024;
https://doi.org/10.1016/j.omtm.2024.101390.

Correspondence: Bangdang Chen, Clinical Medical Research Institute of Xinjiang Medical University, 137 Liyushan South Road, Urumqi 830054, P.R. China.
E-mail: 6357@xjmu.edu.cn

and determines AAV infectivity.[23] Notably, the sPLA2 activity of AAV2 is more pronounced than that of AAV8.[24] So, we constructed a new chimeric AAV8.sPLA2 (AAV8.P) vector in which the sPLA2 of AAV2 was used to replace that of AAV8 in order to enhance the transduction infection efficiency of AAV8.

For this study, we constructed a novel AAV8.P-PCSK9 shRNA (AAV-PCSK9 shRNA) vector containing an shRNA targeting PCSK9 gene that can specifically cross multiple species (mice, rats, and humans). Increasing evidence indicates that extrahepatic PCSK9 has direct effects on atherosclerotic plaques,[25] but we hypothesized that silencing hepatic PCSK9 would mitigate atherosclerosis progression via administration of an AAV-PCSK9 shRNA vector. We found that the PCSK9 levels in liver and plasma were inhibited in AAV-PCSK9 shRNA-transduced C57BL/6J mice, with increased hepatic LDL-R abundance. Next, we used *ApoE*-deficient mice injected with AAV-PCSK9 shRNA and found atherosclerosis mitigation via PCSK9 inhibition and LDL-R abundance increment with inhibition of local and inflammation without systemic lipid changes. These findings indicate that an AAV-PCSK9 shRNA vector may be useful as an effective atherosclerosis therapy.

RESULTS

Superior transduction efficiency and safety of chimeric AAV8.P vector in liver gene therapy

Initially, we investigated the transduction efficiency and potential cytotoxic effects of the innovative chimeric AAV8.sPLA2 (AAV8.P) vector compared with the established AAV8 vector. To assess transduction efficiency and the persistence of transgene expression in liver tissues, we performed a temporal analysis at various time points: 1, 2, and 4 weeks; 3, 6, and 12 months post-administration. Green fluorescent protein (GFP) expression was measured through confocal microscopy (Figures 1A and 1B) and immunoblot analysis (Figure 1C). Notably, GFP expression was observed at 1 week, peaked at 4 weeks, and was maintained for up to 12 months, with AAV8.P achieving a maximum transduction efficiency of approximately 90% at 4 weeks (Figures 1A and 1B). Throughout all evaluated time points, the transduction efficiency of the AAV8.P vector consistently exceeded that of the AAV8 vector, as supported by immunoblot assessments (Figure 1C).

To further elucidate the persistence of transgene expression, we quantified genomic copies of AAV8 and AAV8.P vectors in liver tissue using TaqMan real-time quantitative PCR. The AAV8.P vector consistently demonstrated higher genome copy numbers in the liver compared with AAV8, with significant differences observed from 1 week through 12 months post-administration (Figure 1D). Biodistribution analysis of vector genomes in seven major tissues—liver, heart, spleen, lung, kidney, brain, and muscle—revealed that both AAV8 and AAV8.P exhibited the highest quantities of viral genomes in the liver following tail vein injection, significantly exceeding levels found in other tissues (Figure 1E). Importantly, AAV8.P showed a remarkable 1.55-fold increase in liver genome copies compared with AAV8, while no significant differences were observed in other tissues at 4 weeks post-gene delivery (Figure 1E). These findings confirm the liver's preferential transduction and underscore the superior efficiency of the chimeric AAV8.P vector, indicating its promise as an effective candidate for liver-targeted gene therapy.

In addition to evaluating transduction efficiency, we conducted an extensive assessment of multiple biomarkers indicative of cardiac, hepatic, and renal function at several time points following the administration of the chimeric AAV8.P vector. Our analysis revealed that serum concentrations of lactate dehydrogenase (LDH), creatine kinase (CK), aspartate aminotransferase (AST), alanine aminotransferase (ALT), creatinine, and blood urea nitrogen (BUN) were comparable to those observed in the control group receiving normal saline (Figure S1). This excellent safety profile further supports the potential of AAV8.P for gene therapy applications, particularly in liver-targeted treatments. In summary, the chimeric AAV8.P vector demonstrates superior transduction efficiency and a favorable safety profile compared with the conventional AAV8 vector, highlighting its potential for clinical application in liver-targeted gene therapies.

Chimeric AAV8.P vector effectively targets liver for PCSK9 silencing in C57BL/6J mice

To achieve silencing of PCSK9 in the liver, we designed a new chimeric AAV8.P vector encoding enhanced GFP reporter and anti-PCSK9 shRNA (referred to AAV-PCSK9 shRNA). Male C57BL/6J mice were injected via the tail vein with either AAV-PCSK9 shRNA or the control vector (referred to AAV-GFP) at a dose of 2.0×10^{11} vg/mouse. First, at 4 weeks post-injection, seven major tissues were harvested and analyzed for the tissue tropism and the transduction efficiency by quantifying the GFP-positive areas via direct fluorescence of frozen tissue sections. The histological GFP expression revealed highly efficient liver transductions in mice, with approximately 90% of hepatocytes expressing GFP, but few GFP-positive cells were found in tissues outside the liver for both transduction groups (Figure 2A). These GFP expression results were further validated by PCR (Figure 2B) and western blot analyses (Figures 2C–2E and S2A–S2F). There was no notable difference in GFP expression between the AAV-PCSK9 shRNA and AAV-GFP vectors in the liver. Importantly, GFP expression in non-hepatic tissues was nearly undetectable compared with the liver, both at the mRNA and protein levels in two transduction groups. Overall, the AAV-PCSK9 shRNA vector demonstrated its characteristic liver-tropism, achieving superior transgene expression specifically in murine livers.

Targeted silencing of PCSK9 using AAV shRNA reduces lipid levels without tissue toxicity

We then assessed whether the AAV-PCSK9 shRNA vector effectively promoted silencing of the *PCSK9* gene in C57BL/6J mice. One month after the vector injections, *PCSK9* transcript levels in the liver were reduced by 67% (Figure 3A), circulating PCSK9 protein was reduced by 63% (Figure 3B), and hepatic PCSK9 protein levels were reduced by 50%, resulting in an over 1.5-fold increase in total liver LDL-R protein compared with the levels in mice treated with AAV-GFP (Figures 3F and 3G). Moreover, after overnight fasting, PCSK9

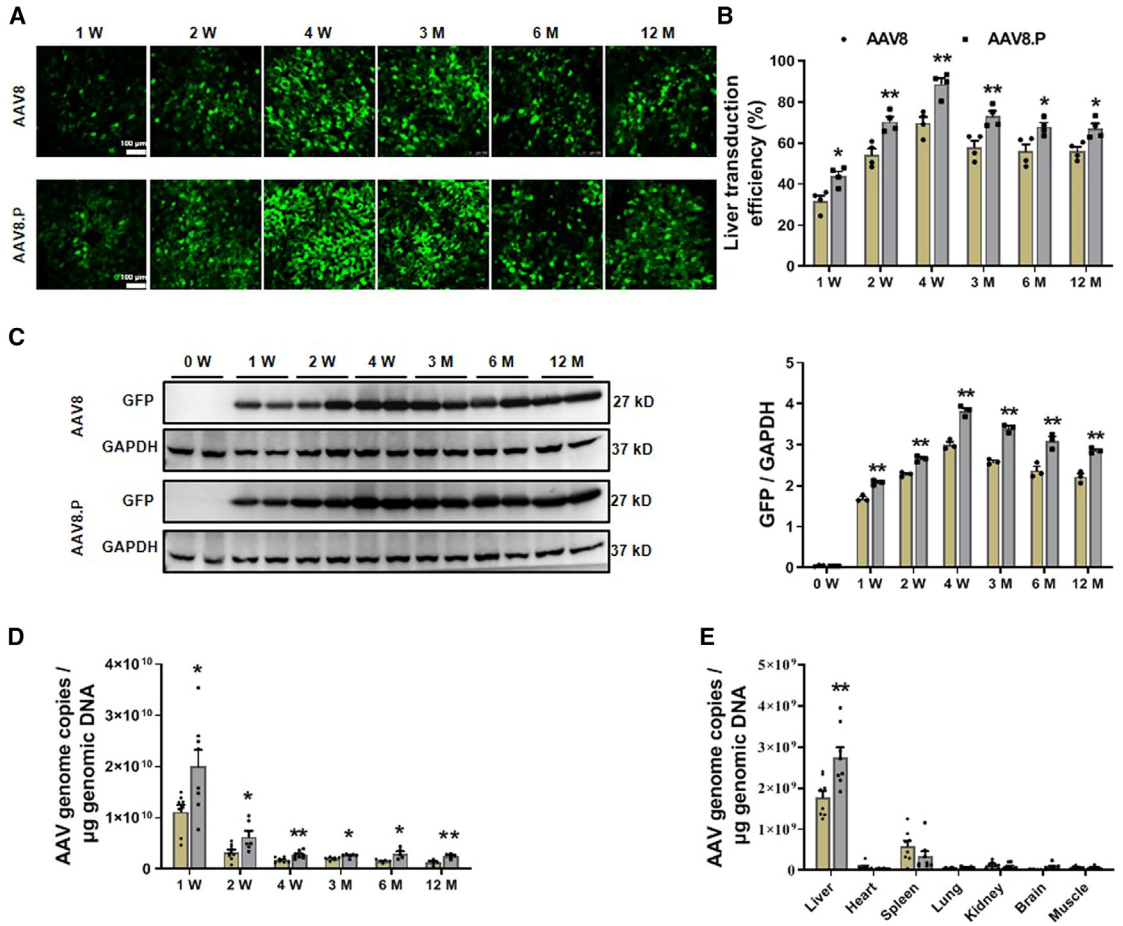

Figure 1. Temporal changes in GFP expression in the liver and biodistribution of AAV8 and AAV8.P vectors in mouse tissues

(A) Representative laser confocal microscopy images showing GFP expression in the liver at various time points (1, 2, 4 weeks and 3, 6, 12 months) following systemic injection of AAV8-GFP or AAV8.P-GFP vectors, scale bar indicates 100 μm. (B) Assessment of gene transduction efficiency in the liver over time following AAV8-GFP or AAV8.P-GFP injection (n = 4/group). Data are shown as means ± SEM. $^{**}p \leq 0.01$, $^{*}p \leq 0.05$ (two-way ANOVA with Bonferroni correction). (C) Western blot analysis of GFP expression levels in liver samples from AAV8 and AAV8.P groups at specified post-delivery time points (n = 3/group). Data are shown as means ± SEM. $^{**}p \leq 0.01$, $^{*}p \leq 0.05$ (two-way ANOVA with Bonferroni correction). (D) qPCR measurement of AAV8 and AAV8.P genome copies in liver tissues at multiple time intervals (1, 2, 4 weeks and 3, 6, 12 months) after injection. Data are shown as means ± SEM. $^{**}p \leq 0.01$, $^{*}p \leq 0.05$ (Unpaired t test). (E) Quantification of AAV genome copies in 1 μg of genomic DNA from heart, liver, spleen, lung, kidney, brain, and skeletal muscle at 4 weeks post-gene delivery, analyzed by qPCR (n = 6–8/group). Data are shown as means ± SEM. $^{**}p \leq 0.01$, $^{*}p \leq 0.05$ (two-way ANOVA with Bonferroni correction).

knockdown was associated with a 34% reduction in serum total cholesterol levels and a 41% reduction in triglyceride concentrations (Figures 3C and 3D).

Simultaneously, we assessed the long-term effectiveness of the AAV-PCSK9 shRNA vector. Our results demonstrated a substantial reduction of 62.3% in circulating PCSK9 protein levels (Figure 3B), which correlated with a 26.5% decrease in total cholesterol (Figure 3C) and a 34.2% reduction in triglycerides (Figure 3D) at the 3-month evaluation. Previous studies have suggested that PCSK9 expression influences ApoB metabolism. Notably, a 50% decrease in hepatic PCSK9 protein levels led to a 59.4% reduction in circulating ApoB levels after 4 weeks (Figure 3E), along with a decreasing trend in hepatic ApoB and Apolipoprotein E (ApoE) protein expression, although this trend did not achieve statistical significance (Figures 3F and 3G).

Reports have indicated potential cellular toxicity associated with shRNA expression,[26,27] To investigate whether systemic administration of AAV-PCSK9 shRNA causes toxicity, we measured serum levels of liver injury biomarkers and conducted a morphological analysis of seven major tissues using hematoxylin and eosin (H&E) staining. One and 3 months post-injection, serum AST and ALT levels showed no significant differences compared with control mice injected with AAV-GFP (Figures 3H and 3I). At the end of the experiment, the seven tissues were collected for H&E analysis (Figure S3). In contrast to the control group, AAV-PCSK9 shRNA administration

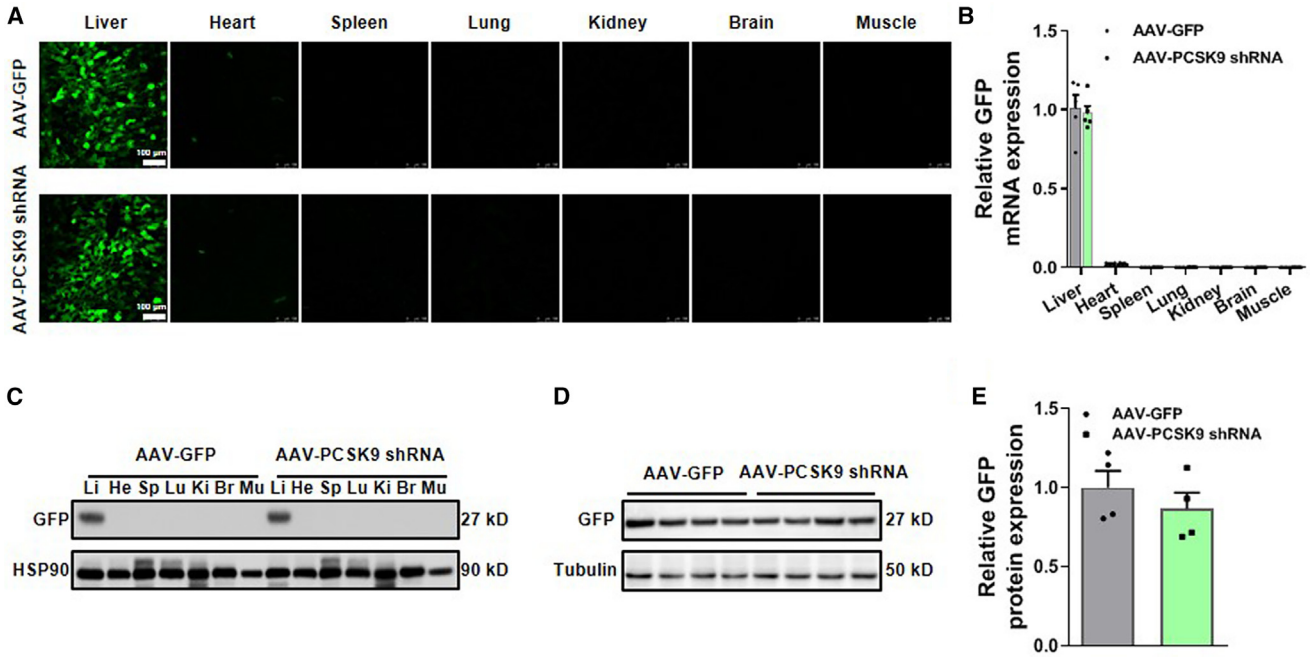

Figure 2. Targeted and robust hepatic gene transduction of GFP utilizing AAV8.P-GFP and AAV8.P-PCSK9 shRNA vectors

(A) Representative images of GFP expression in various tissues obtained through laser confocal microscopy, assessed 4 weeks post systemic administration of AAV-GFP and AAV-PCSK9 shRNA vectors, scale bar indicates 100 μm. (B) Quantitative analysis of GFP mRNA expression performed via real-time PCR across different tissues at 4 weeks following injection of either AAV-GFP or AAV-PCSK9 shRNA vectors. n = 5/group. Data are shown as means ± SEM. Unpaired t test. (C) Detection of GFP expression through western blot analysis in assorted tissues 4 weeks subsequent to gene transfer. Abbreviations: Li, Liver; He, Heart; Sp, Spleen; Lu, Lung; Ki, Kidney; Br, Brain; Mu, Muscle. (D and E) Western blot assessment of GFP expression specifically in the liver 4 weeks following gene transfer. n = 4/group. Data are shown as means ± SEM. Unpaired t test.

did not show significant pathological changes or tissue reactions with the administration of the AAV8.P-PCSK9 shRNA vector over a 3-month period. Taken together, our results demonstrate that AAV8.P-PCSK9 shRNA vector administration achieves targeted and efficient hepatic *PCSK9* mRNA silencing, leading to significant reductions in PCSK9 levels and total plasma cholesterol and triglyceride levels without adversely effecting substantive tissues.

AAV-PCSK9 shRNA silencing in *ApoE*$^{-/-}$ mice induces early changes in lipid profiles but lacks sustained impact on circulating lipids

We used *ApoE*-knockout mice, known to exhibit hyperlipidemia and spontaneously develop advanced lesions, to investigate whether the effect of PCSK9 on plasma lipids is dependent on ApoE. We silenced liver PCSK9 expression with AAV-PCSK9 shRNA in *ApoE*$^{-/-}$ mice fed a chow diet for 6 months. Four weeks post-transduction, hepatic *PCSK9* mRNA expression was significantly reduced by 60% compared with the control group receiving the AAV-GFP vector (Figure 4A). Correspondingly, plasma PCSK9 levels decreased by an average of 37% within 6 months following AAV-PCSK9 shRNA injection (Figure 4B). At the end of the experiment, the hepatic levels of PCSK9 protein were decreased by 36%, leading to a 1.4-fold enhancement in LDL-R protein expression, while ApoB-100 levels remained unchanged (Figure 4E). Despite these changes, serum concentrations of total cholesterol and triglycerides did not show significant alterations at 4 weeks or 6 months post-injection, consistent with prior research indicating that PCSK9 inhibition does not affect plasma lipid levels in *ApoE*$^{-/-}$ mice. However, a notable decrease of 19.4% in serum total cholesterol and a 22.9% reduction in triglyceride levels were observed 2 weeks post-transduction compared with controls (Figures 4C and 4D).

Following vector delivery, we assessed protein expression levels of PCSK9, LDL-R, and ApoB-100 in hepatic tissues at the 2-week mark. Results indicated a 53% reduction in hepatic PCSK9 protein levels, accompanied by a 2.01-fold increase in LDL-R protein expression, while ApoB-100 levels did not change (Figure 4F). Considering previous findings that PCSK9 knockdown reduces ApoB secretion,[28] we measured serum ApoB concentrations in the *ApoE*$^{-/-}$ mice at both 2 weeks and 6 months post-administration. The serum ApoB levels were significantly lower in the group with reduced PCSK9 at 2 weeks, showing a 22.3% decrease, but no significant change was observed at the 6-month mark (Figure 4G).

Additionally, consistent with the reductions in total cholesterol and triglycerides observed at 2 weeks, we noted significant decreases in lipid profiles across various fractions (chylomicrons [CM]/very low-density lipoprotein [VLDL], intermediate-density lipoprotein

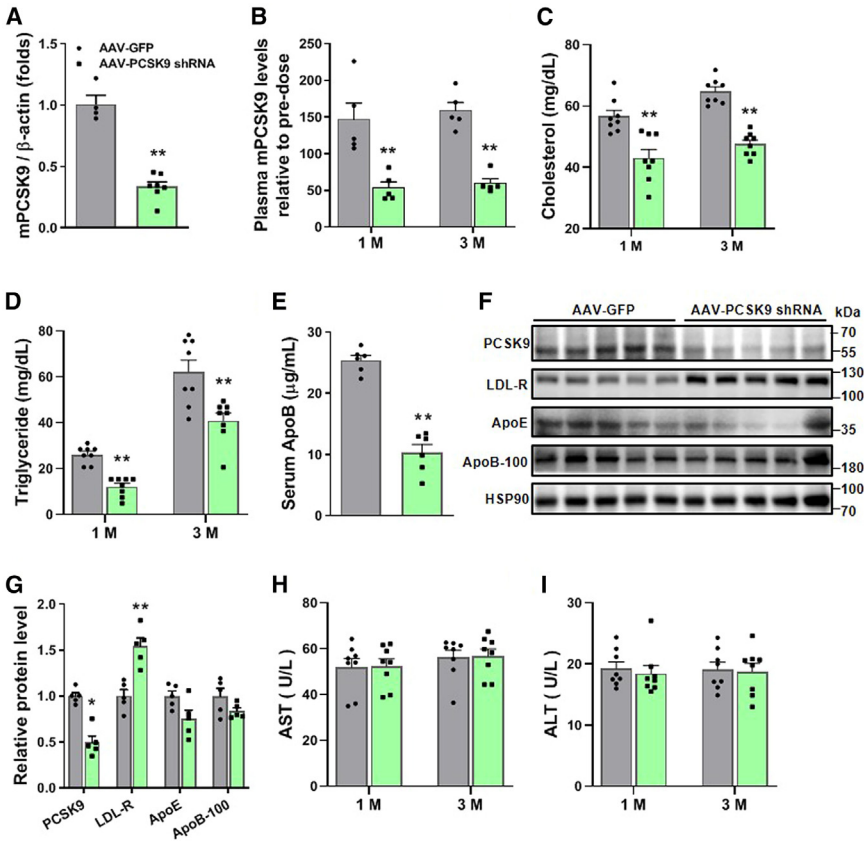

Figure 3. Silencing hepatic PCSK9 leads to decreased serum levels of total cholesterol and triglycerides, without altering AST or ALT concentrations in C57BL/6J mice

(A) Hepatic PCSK9 mRNA levels were quantified using real-time PCR 1-month post-administration of either AAV-GFP or AAV-PCSK9 shRNA, n = 4 for the AAV-GFP cohort and n = 7 for the AAV-PCSK9 shRNA cohort. Data are shown as means ± SEM. $^{**}p \leq 0.01$ (Unpaired t test). (B) Plasma PCSK9 concentrations were assessed through ELISA at 1 and 3 months following transduction with either AAV-GFP or AAV-PCSK9 shRNA, n = 5/group. Data are shown as means ± SEM. $^{**}p \leq 0.01$ (two-way ANOVA with Bonferroni correction). (C and D) Serum levels of total cholesterol and triglycerides were determined 1 month and 3 months subsequent to vector administration, n = 8/group. Data are shown as means ± SEM. $^{**}p \leq 0.01$ (two-way ANOVA with Bonferroni correction). (E) Serum ApoB concentrations (μg/mL) in C57BL/6J mice were measured 1 month after vector administration, n = 6/group. Data are shown as means ± SEM. $^{**}p \leq 0.01$ (Unpaired t test). (F and G) Immunoblot analysis was conducted for hepatic PCSK9, LDL-R, ApoE, and ApoB-100 1 month after vector administration, with corresponding quantification provided in the bar graph, n = 5/group. Data are shown as means ± SEM. $^{*}p \leq 0.05$, $^{**}p \leq 0.01$ (Unpaired t test). (H and I) Plasma aspartate aminotransferase (AST) and alanine aminotransferase (ALT) levels were evaluated at 1 and 3 months post-transduction with either AAV-GFP or AAV-PCSK9 shRNA, n = 8/group. Data are shown as means ± SEM (two-way ANOVA with Bonferroni correction).

[IDL]/LDL, high-density lipoprotein [HDL]) (Figures 4H and 4I). Although we did not detect significantly different total cholesterol and triglyceride levels in AAV-PCSK9 shRNA-transduced mice compared with those in AAV-GFP-transduced mice at the end of the experiment, we observed a trend toward lower LDL-C/LDL-triglyceride and higher high-density lipoprotein-cholesterol (HDL-C)/HDL-triglyceride in the AAV-PCSK9 shRNA-transduced mice. This trend was particularly clear in the VLDL/CM fraction of triglycerides, as indicated by fast protein liquid chromatography (FPLC) analysis (Figures 4J and 4K). Taken together, our findings indicate that silencing PCSK9 in *ApoE*$^{-/-}$ mice alters hepatic PCSK9 and LDL-R levels and causes initial changes in lipid profiles, but does not produce a lasting effect on circulating lipids and ApoB secretion.

PCSK9 silencing reduces atherosclerotic plaque formation and enhances plaque stability in *ApoE*$^{-/-}$ mice

We examined the atherosclerotic lesion areas within the entire aorta tree and the cross-sections of aortic sinus 6 months after the vector injection. In *ApoE*$^{-/-}$ mice transduced with AAV-PCSK9 shRNA, the mean atherosclerotic plaque area was 31.8% smaller than the mean area in AAV-GFP-transduced mice (Figures 5A and 5B). In particular, the lesion areas in the aortic arch and thoracic aorta were significantly lower in the AAV-PCSK9 shRNA-transduced mice (Figures 5C and 5D), without significant differences in the lesion areas of the abdominal and iliac aorta; however, we observed a trend toward smaller areas in the AAV-PCSK9 shRNA-transduced mice (Figures 5E and 5F). Moreover, the lesion areas in cross-sections of aortic sinus were significantly reduced by 27.04% in AAV-PCSK9 shRNA-transduced mice compared with those in AAV-GFP-transduced mice (Figures 5G and 5H). We further investigated the stability of plaques using macrophage CD68 and smooth muscle cell α-SMA markers. Mice with PCSK9 silencing showed enhanced plaque stability, with a 72% reduction in macrophage areas (CD68-positive area, Figures 6A and 6B) and a 52% increase in smooth muscle cell contents (α-SMA-positive area, Figures 6A and 6C). These data suggest that PCSK9 silencing in mice limits the development of atherosclerosis and enhances aortic sinus plaque stability in *ApoE*-deficient mice.

Hepatic PCSK9 silencing reduces local and systemic inflammation in *ApoE*$^{-/-}$ mice

Inflammatory Ly6C^{hi} monocytes/macrophages serve as local inflammation markers in atherosclerotic lesions, and proinflammatory cytokines participate in plaque development. Thus, we evaluated whether hepatic PCSK9 silencing affects the vascular and systemic inflammation responses in *ApoE*$^{-/-}$ mice. PCSK9 silencing reduced Ly6C^{hi} positive cells in aortic sinus by 21.5% lesions ($p < 0.05$) compared

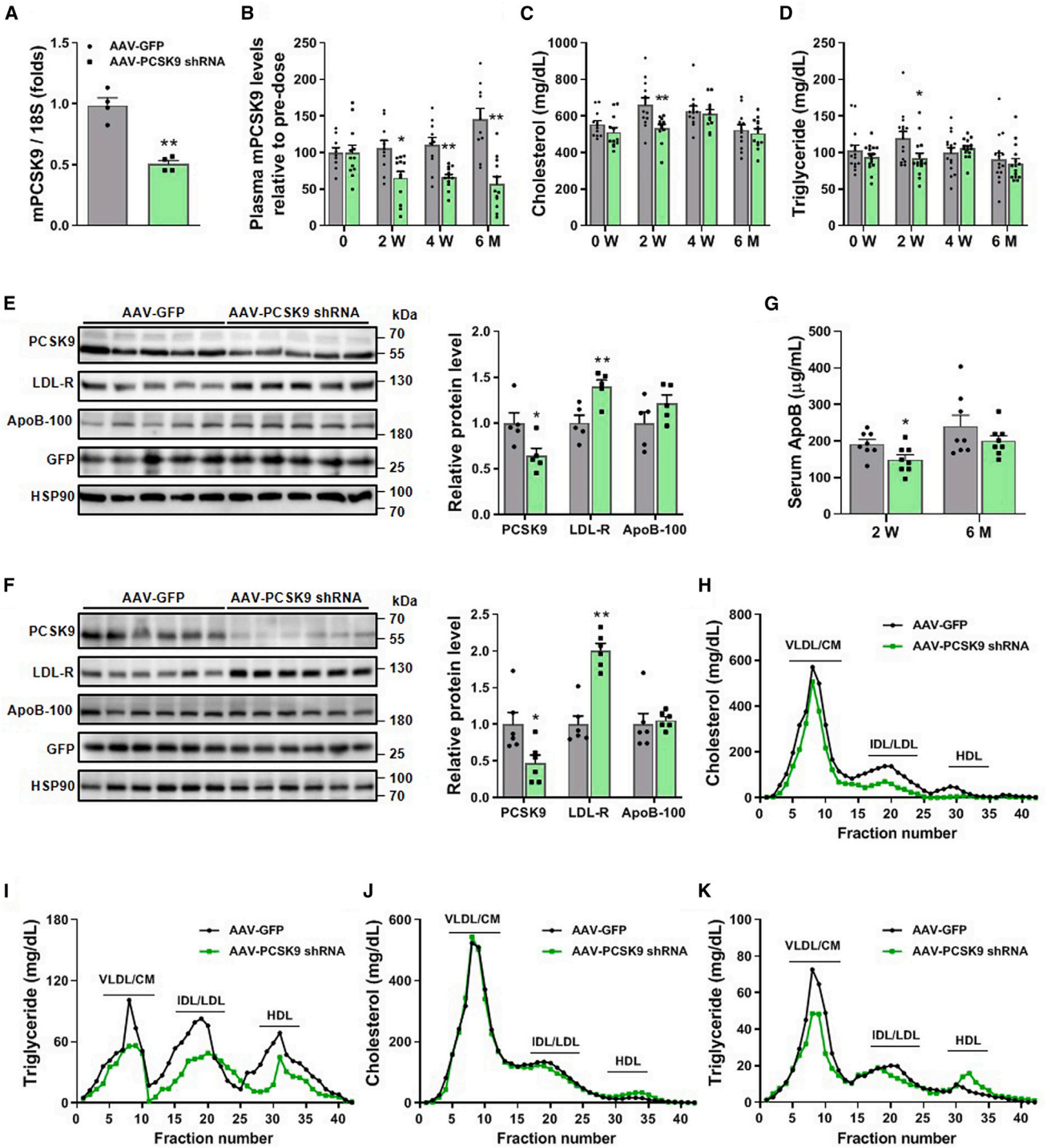

Figure 4. PCSK9 silencing in ApoE$^{-/-}$ mice induces early changes in lipid profiles but lacks a sustained impact on circulating lipids

(A) Hepatic mRNA levels of PCSK9 were quantified using real-time PCR in liver specimens collected 2 weeks post-administration, $n = 4$/group. Data are shown as means ± SEM. $^{**}p \leq 0.01$ (Unpaired t test). (B) Plasma levels of PCSK9 protein were evaluated via ELISA at baseline and at 2 weeks, 4 weeks, and 6 months following injection, $n = 10$ for AAV-GFP, $n = 12$ for AAV-PCSK9 shRNA. Data are shown as means ± SEM. $^{**}p \leq 0.01$ (two-way ANOVA with Bonferroni correction). (C and D) Serum concentrations of total cholesterol and triglycerides were monitored over time after the administration of AAV-PCSK9 shRNA or AAV-GFP, $n = 12$ or 15 per group. Data are shown as means ± SEM. $^{*}p \leq 0.05$, $^{**}p \leq 0.01$ (two-way ANOVA with Bonferroni correction). (E and F) Immunoblotting results depicting hepatic levels of PCSK9, LDL-R, and ApoB-100 proteins at 6 months and 2 weeks post-administration, with corresponding quantification shown on the right, $n = 5$ or 6/group. Data are shown as means ± SEM. $^{*}p \leq 0.05$,

(legend continued on next page)

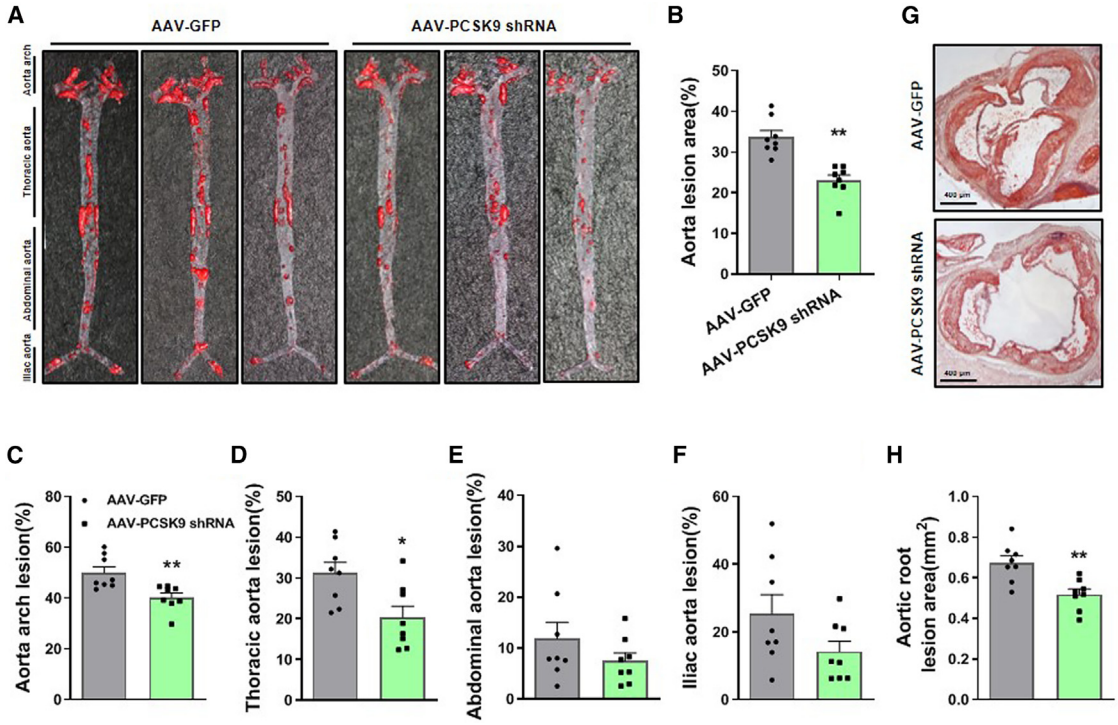

Figure 5. Silencing hepatic PCSK9 protects *ApoE*$^{-/-}$ mice from atherosclerosis development

Twelve-week-old *ApoE*$^{-/-}$ male mice were injected with 2 × 10^{11} viral genomes (v.g.) of AAV-shPCSK9 or AAV-GFP and fed a chow diet for 6 months. (A) Representative Oil Red O-stained images of the *en face* arterial tree. (B–F) Quantification of the lesion areas in (A), n = 8/group. (G) Representative Oil Red O staining in aortic sinus cross-sections, scale bar indicates 400 μm. (H) Quantification of the lesion areas in (G), n = 7 or 8/group. Data are shown as means ± SEM. *$p \leq 0.05$, **$p < 0.01$ (Unpaired t test).

with control mice (Figures 7A and 7B). The mRNA expression levels of *MCP-1*, *TNF-α*, *MIF*, *IL-1β*, and *IL-6* in the aortas were remarkably lower in mice transduced with AAV-PCSK9 shRNA than in control mice (Figure 7C). In addition, the serum concentrations of monocyte chemoattractant protein-1 (MCP-1), tumor necrosis factor (TNF)-α, and macrophage migration inhibitory factor (MIF) were prominently reduced in AAV-PCSK9 shRNA-transduced mice (Figures 7D–7F). Serum concentrations of MCP-1, TNF-α, and MIF were significantly reduced in C57BL/6J mice administered AAV-PCSK9 shRNA vectors over a 3-month period. Notably, MCP-1 levels decreased by 33.5%, MIF by 24.9%, and TNF-α by 34.3% in the AAV-PCSK9 shRNA group compared to the AAV-GFP group (Figures S4A–S4C). These findings underscore the pivotal role of PCSK9 in modulating inflammatory cytokines. These data suggest that hepatic PCSK9 silencing decreased local and systemic inflammation by inhibiting the infiltration of inflammatory Ly6C^{hi}-positive cells into the aortic sinus and reducing the expression and secretion of major proinflammatory cytokines.

DISCUSSION

Herein, we investigated whether AAV-PCSK9 shRNA, based on a novel AAV8.P vector, could serve as a gene therapy delivery system to silence hepatic PCSK9 expression and thereby prevent and mitigate the progression of atherosclerosis. Our results demonstrate that AAV8.P provides superior transduction efficiency and safety, achieving approximately 90% liver transduction and sustaining transgene expression for up to a year. Notably, the AAV-PCSK9 shRNA vector exhibited typical liver-tropism and robust transduction efficiency without inducing unwanted immune responses in hepatic tissue following systemic administration. This vector effectively inhibited hepatic *PCSK9* transcription, reduced protein expression, and lowered circulating PCSK9 levels. Furthermore, it increased LDL receptor levels, reduced ApoB concentrations, and lowered total cholesterol and triglyceride levels in C57BL/6J mice. In *ApoE*-deficient murine models, while transduction with the AAV-PCSK9 shRNA vector enhanced plaque stability, it did not produce sustained changes in circulating lipid levels,

**$p \leq 0.01$ (Unpaired t test). (G) Serum ApoB levels (μg/mL) were assessed in mice at 2 weeks and 6 months post-administration of AAV-GFP or AAV-PCSK9 shRNA, n = 8/group. Data are shown as means ± SEM. *$p \leq 0.05$ (Unpaired t test). (H and I) Fast protein liquid chromatography (FPLC) profiles of cholesterol and triglycerides were analyzed from pooled serum collected 2 weeks post-administration. (J and K) FPLC assessment of cholesterol and triglyceride profiles in pooled serum at 6 months post-administration.

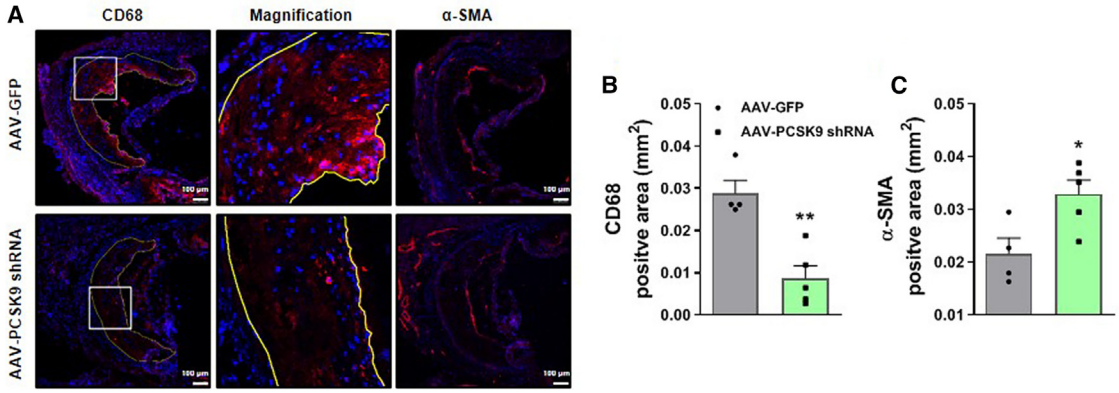

Figure 6. Silencing PCSK9 improves plaque stability in aortic sinus lesions

(A) Representative images of macrophages and smooth muscle cells by immunostaining with CD68 antibody (red) and α-smooth muscle actin antibody (red) in aortic sinus lesions, scale bar indicates 100 μm, plaque areas circled with yellow solid lines. (B) Quantification of macrophage-positive areas in (A), $n = 4$ or 5/group. (C) Quantification of smooth muscle cell-positive areas in (A). $n = 4$ or 5/group. Data are shown as means ± SEM. $^{*}p \leq 0.05$, $^{**}p < 0.01$ (Unpaired t test).

such as total cholesterol and triglycerides. However, during the initial 2 weeks of treatment, it significantly reduced serum levels of total cholesterol, triglycerides, ApoB, and other atherogenic lipoproteins. Furthermore, AAV-PCSK9 shRNA mitigated atherosclerotic development by decreasing inflammatory cell infiltration in aortic tissues and reducing circulating inflammatory cytokines. Collectively, these findings underscore the potential of the AAV8.P-PCSK9 shRNA vector as an effective gene therapy delivery system for the prevention and treatment of atherosclerosis, illustrating its promise in addressing cardiovascular disease through targeted gene silencing.

AAV vectors are increasingly being utilized in research trials to address hepatic hereditary disorders.[29] A critical factor influencing the infectivity of these viral vectors is the activity of the secreted phospholipase A2 (sPLA2) protein associated with the capsid. In our study, we developed a novel chimeric vector, AAV8.P, by substituting the sPLA2 domain of AAV8 with that of AAV2, aiming to harness AAV2's superior sPLA2 activity to enhance gene delivery efficiency. Our results demonstrated that the AAV8.P vector significantly improved transfection rates in the liver compared with AAV8, achieving efficiencies of 89% vs. 70% at 4 weeks and 67.2% vs. 56.1% at 12 months following a single tail vein injection at equivalent dosages. Both AAV8.P and AAV8 were predominantly localized in the liver, with lower concentrations in other organs, consistent with previous findings by Wang et al.[30] Importantly, the genome copy number of AAV8.P in the liver consistently exceeded that of AAV8 throughout the 12-month observation period. Safety evaluations from clinical trials have reported no significant adverse events associated with AAV vectors, aside from transient increases in aminotransferase levels.[31–33] Our findings support this, as parameters for heart, liver, and kidney function in mice remained within the normal range during the transduction of AAV8.P or AAV8 compared with the saline control group. These results underscore the potential of AAV8.P as a more effective and safer vector for liver gene therapy, paving the way for advancements in the treatment of hepatic disorders.

PCSK9, a key determinant of cholesterol homeostasis, is mainly expressed in the liver, making it an attractive therapeutic target for hypercholesterolemia. While three monoclonal antibodies and one small interfering RNA (siRNA) have received regulatory approval, their limitations underline the need for innovative approaches that provide sustained efficacy. Monoclonal antibodies primarily inhibit the secreted form of PCSK9 and necessitate frequent administration—monthly or bi-monthly injections—to maintain therapeutic effects. In contrast, our study introduces AAV-PCSK9 shRNA, which exerts its impact by silencing PCSK9 at both the transcriptional and translational levels, affecting not only secretion but also intracellular trafficking and degradation of the protein. Frank-Kamenetsky et al. demonstrated that lipid nanoparticle-encapsulated siRNA (LNP-PCS-A2) targeting PCSK9 can significantly reduce hepatic PCSK9 mRNA levels by 60%–70% and total cholesterol by 30% in C57BL/6 mice within 3 days at a dose of 5 mg/kg.[34] However, the effect on PCSK9 mRNA was transient, lasting about 20 days, with similar observations in rat models, where cholesterol levels decreased for only 10 days before returning to baseline by day 21. In contrast, our study using AAV-PCSK9 shRNA achieved a more sustained effect, demonstrating a 67% reduction in hepatic PCSK9 synthesis and resulting in a 34% decrease in total cholesterol and a 41% decrease in triglycerides 1-month posttreatment in C57BL/6J mice. Notably, circulating PCSK9 levels decreased by 62.3%, with cholesterol and triglyceride reductions of 26.5% and 34.2%, respectively, sustained over 3 months. Remarkably, 6 months after AAV-PCSK9 shRNA administration, plasma PCSK9 concentrations in *ApoE*-knockout mice remained 60% lower compared with the AAV-GFP cohort, demonstrating the long-lasting therapeutic benefits of AAV-PCSK9 shRNA compared with existing non-gene therapy methods. Additionally, the AAV8.P-PCSK9 shRNA vector offers

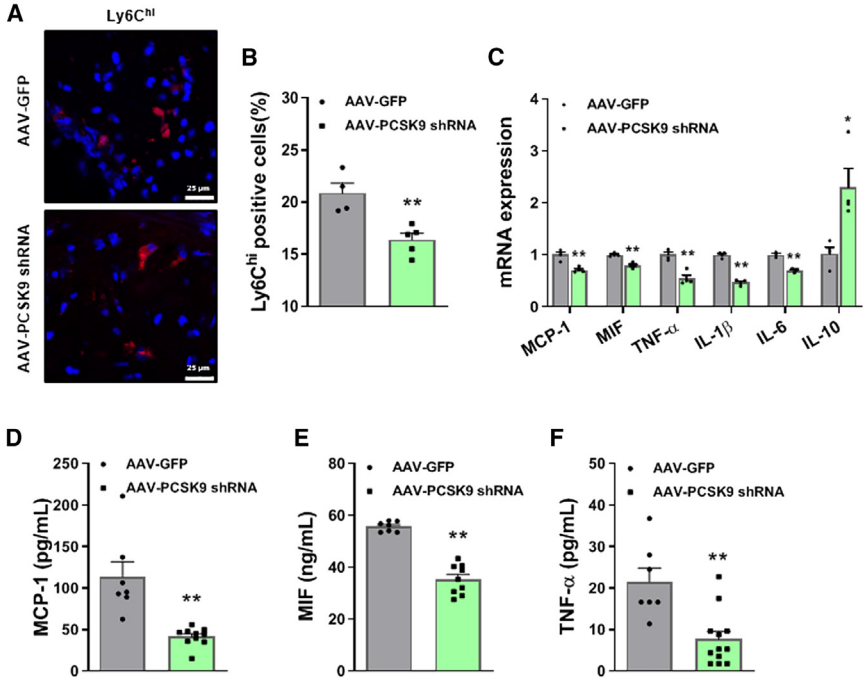

Figure 7. Silencing PCSK9 attenuates atherosclerotic aorta and serum inflammatory monocyte infiltration and inflammatory gene expression in *ApoE*$^{-/-}$ mice

(A) Representative images and quantification (B) of Ly6C^{hi}-positive cells via aortic sinus lesions immunostaining, scale bar indicates 25 μm, n = 4 or 5/group. (C) Real-time PCR analysis of *MCP-1*, *TNF-α*, *MIF*, *IL-1β*, *IL-6*, and *IL-10* mRNA expression in aortas from AAV-transduced *ApoE*$^{-/-}$mice fed a chow diet for 6 months, n = 3 or 4/group. (D–F) Serum levels of MCP-1, MIF, and TNF-α from AAV-transduced *ApoE*$^{-/-}$mice fed a chow diet for 6 months via ELISA, n = 7–12/group. Data are shown as means ± SEM. *$p \leq 0.05$, **$p < 0.01$ (Unpaired t test).

significant advantages in terms of administration frequency. Unlike monoclonal antibodies and inclisiran, which require repeated dosing, our AAV8.P vector can maintain transgene expression for up to a year. This extended duration not only enhances patient adherence but also has the potential to reduce overall healthcare costs by minimizing the need for frequent treatments. Therefore, our findings highlight the durability and long-term efficacy of AAV-PCSK9 shRNA as a novel cholesterol management strategy. AAV8.P-based methods may provide a more effective means of ensuring sustained lipid control.

Our findings align with previous research indicating that PCSK9 deletion does not significantly affect total cholesterol levels in *ApoE*-knockout mice. Specifically, studies have shown that *ApoE*-knockout mice with PCSK9 deletion maintained comparable total cholesterol levels to control mice on a regular chow diet over 6 months.[35] Similarly, Tang et al. found that administering PCSK9 shRNA via lentivirus had no impact on plasma total cholesterol or triglyceride levels in *ApoE*$^{-/-}$ mice fed a 2% cholesterol diet.[36] In our study, PCSK9 knockdown in *ApoE*$^{-/-}$ mice also failed to change total cholesterol or triglyceride levels at the 6-month endpoint. Interestingly, despite these unchanged lipid levels, we observed that AAV-PCSK9 shRNA administration inhibited the levels of apoB-containing lipoprotein particles, leading to a decreasing trend in serum ApoB-100 levels. Notably, 2 weeks post-injection, AAV-PCSK9 shRNA administration resulted in significant reductions in various lipoprotein particle levels, including chylomicrons (CM/VLDL), intermediate-density lipoproteins (IDL/LDL), and high-density lipoproteins (HDL). At this time point, serum total cholesterol, triglycerides, and ApoB-100 levels were also significantly lower in treated mice compared with controls. These findings suggest that while PCSK9 knockdown may not directly alter total cholesterol or triglyceride levels in the context of *ApoE*-knockout mice, it does have a profound impact on the composition and levels of lipoprotein particles. This highlights the complex role of PCSK9 in lipid metabolism and suggests potential therapeutic implications for targeting PCSK9 in conditions characterized by dyslipidemia.

Whether PCSK9 affects the development of atherosclerotic plaques in *ApoE*$^{-/-}$ settings has been unclear. Some studies suggest that PCSK9 deficiency does not influence atherosclerotic lesion size. For instance, one study found that PCSK9 deficiency did not affect atherosclerotic lesion size in *ApoE*$^{-/-}$ mice,[37] while Denis et al. reported that PCSK9 deletion did not reduce aortic root plaque sizes but significantly decreased cholesterol ester levels in the whole aorta,[35] indicating that PCSK9 deficiency may protect *ApoE*$^{-/-}$ mice from atherosclerosis. In contrast, another study demonstrated that PCSK9 silencing via lentivirus-mediated PCSK9 shRNA transduction markedly limited atherosclerosis development in *ApoE*$^{-/-}$ mice fed a high cholesterol diet.[36] In our study, we found that transduction with AAV8.P-PCSK9 shRNA resulted in a more than 30% decrease in lesion sizes in the entire aortic tree and aortic sinus of *ApoE*$^{-/-}$ mice. This decrease in atherosclerotic burden was accompanied by significant reductions in triglyceride profiles and a trend toward lower serum ApoB-100 levels, particularly in triglyceride-rich lipoproteins such as VLDL. The atherogenic role of ApoB and its associated lipoproteins[38,39] has been increasingly emphasized in the context of cardiovascular risk.[40,41] Furthermore, Sun et al. demonstrated that hepatic reduction of PCSK9 influences atherogenesis by modulating the levels and characteristics of ApoB-containing lipoproteins.[28] Our results support these findings by showing that AAV-PCSK9 shRNA administration effectively reduced PCSK9 levels, resulting in significant decreases in serum ApoB levels in both C57BL/6J mice after 1 month and *ApoE*$^{-/-}$ mice after 2 weeks. Additionally, our results indicate

that hepatic reduction of PCSK9 enhances LDL receptor levels, promoting the clearance of LDL particles and contributing to the observed decrease in atherosclerosis. Our study supports the notion that PCSK9 serves as a crucial regulator of atherosclerosis in *ApoE*$^{-/-}$ mice, highlighting the potential of targeting this protein through AAV-PCSK9 shRNA as an effective therapeutic approach for managing hyperlipidemia and atherosclerotic disease in cardiovascular contexts.

Atherosclerosis is a chronic inflammatory disease of arteries characterized by the presence of inflammatory cytokines. Increasing evidence has shown a direct link between PCSK9 and atherosclerotic inflammation.[42] Macrophages are involved in the inflammatory response in plaques, and the content and polarization state of these cells in plaques have a role in the progression of atherosclerotic lesions.[43] Ly6Chi monocytes are proposed to be precursors of proinflammatory M1 macrophages. Tang et al. reported that PCSK9 knockdown via LV-PCSK9 shRNA inhibits atherosclerosis by decreasing vascular inflammation and resulting in fewer CD68-positive macrophages and reduced expression of vascular inflammation regulators such as MCP-1, interleukin (IL)-1β, and TNF-α in ApoE-knockout mice.[36] Conversely, transgenic human PCSK9 locally promoted infiltration of Ly6C^{hi} monocytes within atherosclerotic lesions in *ApoE*-knockout mice.[44,45] Increasing evidence suggests that PCSK9 affects arterial wall and systemic inflammation. PCSK9 inhibition by AT04A vaccine or alirocumab reduced the number of monocytes in plaques,[46,47] and AT04A decreased the plasma levels of inflammatory cytokines, including macrophage inflammatory protein-1β, macrophage-derived chemokine, cytokine stem cell factor, and vascular endothelial growth factor A, in *ApoE* *3Leiden.CETP mice. In our study, *ApoE*-knockout mice transduced with AAV8.P-PCSK9 shRNA exhibited a dramatic decrease in their plaque areas and plasma levels of MIF, MCP-1, and TNF-α. TNF-α has multiple roles during atherosclerosis development, promoting endothelial dysfunction and recruiting and inducing proliferation of monocytes/macrophages.[48] MIF, an inflammatory cytokine,[49] is another pivotal mediator of atherosclerotic lesion formation.[50] In *ApoE*-deficient mice, MIF deletion reduced monocyte recruitment, macrophage content, and smooth muscle cell proliferation into plaques, markedly mitigating atherogenesis.[51] MIF blockade with neutralizing antibodies in *ApoE*-knockout mice resulted in a regression of atherosclerotic plaques with fewer infiltrating macrophages.[52] MCP-1 is a key chemokine in atherosclerosis, regulating migration and infiltration by monocytes/macrophages.[53] Our results revealed that the low levels of these plasma proinflammatory cytokines were accompanied by reduced proinflammatory Ly6C^{hi} monocytes in the plaques. Therefore, it seems possible that low levels of these proinflammatory cytokines in circulating blood may have inhibited the infiltration of proinflammatory Ly6C^{hi} monocytes into the plaques. In addition to the decrease in the number of the proinflammatory Ly6C^{hi} monocytes, the CD68-positive area of plaque macrophages was more significantly reduced in AAV8.P-PCSK9 shRNA-transduced mice than in control mice. Importantly, AAV8.P-PCSK9 shRNA-transduced mice exhibited a more stable plaque morphology with a less inflammatory phenotype, reduced levels of proinflammatory cytokine mRNAs (including *MIF*, *MCP-1*, *TNF-α*, *IL-1β*, and *IL-6* mRNA) and increased anti-inflammatory cytokine mRNA (*IL-10*) than control mice. Taken together, these data suggest that silencing hepatic PCSK9 by AAV8.P-PCSK9 shRNA transduction in mice resulted in atherosclerotic plaque mitigation, with systemic and vascular inflammation reduction in *ApoE*-knockout mice.

To the best of our knowledge, this is the first study reporting on the anti-atherosclerotic effects of AAV8.P-PCSK9 shRNA, a gene therapy delivery system based on AAV8.P vectors. We are aware of the limitations of our study, particularly when regarding human translation applications: The optimal length of treatment with AAV8.P-PCSK9 shRNA remains unclear, but the treatment may need to be initiated early given the Mendelian randomization results showing the effects of long-term exposure to high LDL-C on the risk of ASCVD.[54] Also, in addition to the experiments in *ApoE*$^{-/-}$ mice that develop atherosclerosis spontaneously, studies on well-established mouse models such as *ApoE* *3Leiden.CETP mice,[55] which closely mimic atherosclerosis initiation and development in humans, and in transgenic human PCSK9 mice, as well as in rhesus monkeys are needed to verify our findings. Ultimately, our investigation focused on a single shRNA due to constraints in funding and scope. While this approach provided initial insights, testing a broader range of shRNAs would enhance the robustness of our findings.

In conclusion, AAV8.P-PCSK9 shRNA injection resulted in long-term inhibition of hepatic PCSK9 transcription and expression. This strategy may be useful as an alternative gene therapy delivery system to reduce atherosclerotic inflammation through both lipid-dependent and lipid-independent pathways that may help promote substantial atherosclerotic plaque reversal.

MATERIALS AND METHODS

Virus vector preparation

The AAV8.sPLA2 vector was engineered to enhance the gene delivery capabilities of the AAV8 serotype by incorporating the phospholipase domain from AAV2. Specifically, the first 132 amino acids of the VP1 protein of AAV8 were replaced with the corresponding sequence from AAV2, resulting in the generation of the AAV8.sPLA2 (AAV8.P) vector. The plasmid construction and viral vector production were performed by Virovek (Hayward, CA, USA). Two oligos corresponding to PCSK9 shRNA were synthesized (5′-3′sense strand: GATCCGCCTGGAGTTTATTCGGAATCA AGAGTTCCGAATA AACTCCAGGCAGTTTTTTG, 5′-3′antisense strand : TCGACAA AAAAC TGCCTGGAGTTTATTCGGAACTCTTGATTCCGAATA AACTCCAGGCG). Both oligos were phosphorylated and mixed in one tube to anneal them together, the resulting fragment was cut with with SalI and BamHI and ligated to the SalI and BamHI sites of pFB-CBA-GFP-Scrambled to create pFB-CBA-GFP-PCSK9 shRNA. Recombinant adeno-associated viral (AAV) vectors were produced based on the AAV8.P vector. These vectors encoded either PCSK9-shRNA and a GFP reporter (designated as AAV-PCSK9 shRNA) or a control scrambled shRNA driven by a U6 promoter along with a GFP reporter (designated as AAV-GFP). Both AAV8

and AAV8.P vectors were packaged using single-stranded DNA containing an enhanced green fluorescent protein (GFP) gene, which was regulated by the constitutive chicken β-actin promoter with a CMV enhancer (AAV8-CBA-GFP and AAV8.P-CBA-GFP). All AAV vectors were produced utilizing a recombinant baculovirus (rBac) system in SF9 cells, as previously described in the literature.[56] Vector titers for all four AAV constructs were determined using quantitative polymerase chain reaction (qPCR). Primers specific to the CMV enhancer region were utilized for accurate quantification.

Animal models

Male C57BL/6J and *ApoE*$^{-/-}$ mice were purchased from the Shanghai Model Organisms Center (Shanghai, China) and housed at the Xinjiang Medical University Medical Laboratory Animal Center. The mice in our study were fed a normal chow diet. All experiments involving animals were conducted in accordance with the guidelines of the Ethics Committee of the First Affiliated Hospital of Xinjiang Medical University.

To evaluate the transduction efficiency and potential cytotoxicity of the novel chimeric AAV8.P vector compared with the conventional AAV8 vector, male C57BL/6J mice (8–10 weeks old) were randomized into three groups: normal saline (n = 30), AAV8 (n = 40), and AAV8.P (n = 40). Mice received a tail vein injection of 200 μL containing 2×10^{11} particles of either AAV8, AAV8.P, or saline. The mice were subsequently euthanized, and samples were collected at 1, 2, and 4 weeks, as well as at 3, 6, and 12 months post-injection.

To assess the effectiveness of the AAV-PCSK9 shRNA vector in silencing the PCSK9 gene, male C57BL/6J mice were injected via the tail vein with either AAV-GFP or AAV-PCSK9 shRNA at equal doses as described above. Mice from both groups (n = 18/group) were euthanized at 4 and 12 weeks post-injection.

To assess the therapeutic efficacy of the AAV-PCSK9 shRNA vector in mitigating hyperlipidemia and advanced atherosclerotic lesions in the context of *ApoE* gene deficiency, the *ApoE*$^{-/-}$ mice (12 weeks old) were randomly injected with either AAV-GFP or AAV-PCSK9 shRNA via the tail vein at the same doses as described above. Blood was collected from the retro-orbital plexus after administering isoflurane anesthesia at 0, 2, and 4 weeks, as well as at 6 months after the AAV injection, to measure total cholesterol, triglycerides, lipoprotein profiles, and serum PCSK9 levels. At the end of the experiments, the mice were euthanized, and aortas and liver samples were harvested.

Fluorescent imaging

We assessed the biodistribution of the injected vectors *in vivo* via fluorescent imaging of GFP expression in various mouse organs as published.[57] Briefly, fresh organs and tissues were fixed in 4% paraformaldehyde for 4 h at room temperature, triple washed in phosphate-buffered saline (PBS) for 5 min each time, and then dehydrated with 15% sucrose in PBS at 4°C overnight. All samples were immediately embedded in OCT and snap-frozen. Fresh frozen samples were sliced into 4-μm-thick sections. We acquired 8–10 fluorescent images of each tissue section using a Leica TCS SP8 laser confocal scanning microscope (Leica TCS SP8, Mannheim, Germany) at ×20 magnification, along with corresponding bright field images.

Western blotting

Liver tissues were homogenized in RIPA lysis and extraction buffer (Thermo Scientific, Rockford, IL, USA) containing a protease inhibitor cocktail (1:200, ab201111, Abcam). After sonication and incubation for 15 min on ice, the lysates were centrifuged at 13,000 × g for 15 min at 4°C. We quantified the protein in the samples using a Pierce BCA Protein Assay Kit (Thermo Scientific, Rockford, IL, USA). Protein samples were boiled in NuPAGE LDS Sample buffer (Thermo Scientific, Rockford, IL, USA) for 8 min and then separated in NuPAGE 4%–12% Bis-Tris Gel electrophoresis before being transferred onto polyvinylidene difluoride transfer membrane (Millipore, Billerica, MA, USA). After being blocked with 5% skim milk in TBST for 1 h at room temperature, the membranes were incubated with primary antibodies targeting LDL-R (1:1,000, ab52818, Abcam), GFP (1:1000, 2956S, Cell Signaling Technology), ApoE (1:500, K23100R, Meridian life science), Apo-B48/100 (1:500, K23300R, Meridian life science), Mouse PCSK9 (1 μg/mL, AF3985, R&D), β-actin (1:1,000, 4970S, Cell Signaling Technology), GAPDH (1:1000, 5174, Cell Signaling Technology), α-Tubulin(1:1000, ab4074, Abcam), and HSP90 (1:1,000, 4874S, Cell Signaling Technology), followed by incubation with the corresponding secondary antibody conjugated with horseradish peroxidase goat anti-rabbit immunoglobulin (Ig)G (1:3,000, ab205718, Abcam) or horseradish peroxidase rabbit anti-goat IgG (1:1,000, SA00001-4, Proteintech) for 1 h at room temperature. We detected specific bands using enhanced chemiluminescence reagent (Millipore, Waltham, MA, USA) and determined protein levels by densitometry analysis using the Image Lab 4.0 software (Bio-Rad Laboratories, Hercules, CA, USA).

En face oil red O staining of the arterial tree

For quantification of the atherosclerotic lesion areas, we stained the arterial tree from aorta arch to iliac arteries with oil red O as published with modifications.[58] Briefly, the arterial trees were dissected, opened longitudinally to expose the atherosclerotic plaques, rinsed in saline, and fixed in 4% paraformaldehyde for 10 min. We stained the fixed arterial trees with freshly prepared 0.3% oil red O solution (3:2, O1391, Sigma) at 45°C for 8 min, and then de-stained them with 75% alcohol for 8 min. The stained arterial trees were flattened on soaked black absorbent paper and photographed using a digital camera. We quantified the atherosclerotic lesions stained in red using the ImageJ software as a percentage of the total aorta area.

Analysis of atherosclerotic lesions

For microscopic analysis of atherosclerotic plaques in aortic sinuses, we prepared cryopreserved cross-sections of aortic sinus as published.[58] Briefly, the aortic sinuses were harvested by trimming the bottom half of the hearts carefully along a plane parallel to the atria, and then embedding the specimens in a Tissue-Tek OCT cryostat mold. Serial 8-μm-thick cross-sections were sliced and stored at −80°C. Sections of aortic sinus were stained with oil red O and

Table 1. Primer sequences for PCR

Genes	Forward primers	Reverse primers
MCP-1	5′-CTGCATCTGCCCTAAGGTCT-3′	5′-AGTGCTTGAGGTGGTTGTGG-3′
TNF-α	5′-AGCATCTCCACTCCGTCCT-3′	5′-AGCACCCAAAGTCACCAAGT-3′
IL-6	5′-GCTACCAAACTGGATATAATCAGGA-3′	5′-CCAGGTAGCTATGGTACTCCAGAA-3′
IL-1β	5′-AGGAGAACCAAGCAACGACA-3′	5′-GCTTGGGATCCACACTCTCC-3′
mPCSK9	5′-TATCCCAGCATGGCACCAGA-3′	5′-ATGGTGACCCTGCCCTCAA-3′
MIF	5′-TAGACCACGTGCTTAGCTGAGCC-3′	5′-GCCCAGCTGGAGCACACTATT-3′
IL-10	5′-ACCTGGTAGAAGTGAATGCCC-3′	5′-GGAGAAATCGATGACAGCGCC-3′
18S	5′-TTGACGGAAGGGCACCACCAG-3′	5′-GCACCACCACCCACGGAATCG-3′

counterstained with hematoxylin. We calculated the areas of atherosclerotic plaques in the aortic root after adjusting the measurements for pixel size.

To perform immunofluorescence staining of the aortic root samples, we incubated the sections with primary antibodies for CD68 antibody (1:200, MCA1957, AbD Serotec), α-smooth muscle actin (1:100, 14395-1-AP, Proteintech), or Ly6C antibody (1:100, 14-5931-82, eBioscience), followed by incubation with Alexa Fluor 546 goat anti-rat IgG (1:500, A11081, Invitrogen) or Alexa Fluor 594 donkey anti-rabbit IgG (1:400, A21207, Invitrogen), as appropriately, and counterstaining with 4′,6-diamidino-2-phenylindole (DAPI) to color nuclei.

We captured three images covering the whole aortic root sections using a laser confocal scanning microscope (Leica TCS SP8, Mannheim, Germany) at ×10 magnification for quantitative analysis of macrophages and smooth muscle cells. The lesion areas containing macrophages and smooth muscle cells were quantified using the ImageJ software and expressed as the percentage of the total lesion area. For quantitative analysis of inflammatory monocytes, we captured three to five random fields at ×40 magnification and calculated the percentage of total cells in each field.

Enzyme-linked immunosorbent assays

We measured plasma mouse PCSK9 levels using a mouse Quantikine ELISA Kit (catalog number, MPC900; R&D Systems, Minneapolis, MN) according to the manufacturer's instructions. Mouse MIF serum levels were measured using an MIF ELISA Kit (catalog number, E0698m; EIAab, Wuhan, China). In addition, we quantified the mouse serum levels of MCP-1 and TNF-α using ELISA kits (catalog numbers, BMS6005 and BMS607/3; Invitrogen, USA). Plasma apoB levels were quantified by Mouse Apo B SimpleStep ELISA Kit (catalog numbers, ab230932; Abcam, UK).

Total cholesterol and triglyceride levels

After overnight fasting, blood samples were collected and centrifuged at 3,000 rpm for 15 min at 4°C. Equal-volume 50-μL serum samples from 10 mice were pooled, and the combined serum was separated using fast protein liquid chromatography (FPLC) on a Superose 6 column (GE Healthcare) and eluted in PBS at a constant flow rate of 0.4 mL/min into 42 fractions. The concentrations of TC and triglyceride in the original sera or the FPLC fractions were enzymatically measured using kits (catalog numbers, 294–65801 and 290–63701; Wako Pure Chemical Industries, Osaka, Japan).

Quantitative real-time PCR analysis

Total RNA samples were extracted from liver or the arterial tree of mice using TRIzol reagent (Invitrogen, Carlsbad, CA, USA). We used 2 μg of total RNA as a template to synthesize cDNA using the FastKing RT Kit (catalog number, KR116; TIANGEN BIOTECH, Beijing, China). The quantitative real-time PCR was run on a QuantStudio 6 Flex System (Applied Biosystems) using a SuperReal PreMix Color (SYBR Green) reagent (catalog number, FP215; TIANGEN BIOTECH, Beijing, China). Each PCR reaction was amplified in duplicate. We calculated relative expression levels using the comparative $2^{-\Delta\Delta CT}$ method normalized to *18S* as an internal control. Table 1 lists the primer sequences.

TaqMan real-time fluorescence quantitative PCR

To examine the copy numbers of AAV8 or AAV8.P in various mouse tissues, genomic DNA was extracted at a final concentration of 100 ng/μL using the QIAGEN Genomic DNA Extraction Kit (Biotech, Shanghai, China). Known copy numbers of the plasmid pFB-CMV-GFP from Virovek (Hayward, CA, USA) were used to construct the standard curve. The following primers were used for amplifying GFP: 5′ AACGAGAAGCGCGATCACAT 3′ (forward primer) and 5′ AACGAGAA GCGCGATCACAT 3′ (reverse primer). The probe sequence, CGGCGGTCACGAACTCCAGCA, was synthesized by Invitrogen. The 20-μL reaction system for quantitative PCR was as follows: 1 μL (100 ng) of genomic DNA, 0.8 μL (0.4 μM) of upstream and downstream primers, 0.8 μL (0.4 μM) of probe, 10 μL of 2× GoldStar probe mixture, and 6.6 μL of ultrapure water. The reaction conditions included UNG enzyme digestion at 37°C for 10 min, pre-denaturation at 95°C for 10 min, followed by 40 cycles of denaturation at 95°C for 15 s and annealing/extension at 60°C for 1 min. Quantitative PCR was conducted on an ABI 7900 (Applied Biosystems, Foster City, CA, USA). Each sample was run in triplicate. The results were expressed as mean AAV vector genome copy numbers per microgram of genomic DNA in various tissues, according to the standard curve equation.

Biochemical assays

Plasma levels of aspartate aminotransferase (AST) and alanine aminotransferase (ALT) were measured for liver toxicity; lactate dehydrogenase (LDH) and creatine kinase (CK) were measured for cardiac toxicity; and creatinine and blood urea nitrogen (BUN) were assessed for renal function using an automatic biochemical analyzer (HITACHI 7600, Tokyo, Japan).

Hematoxylin and eosin staining

We used a 4% paraformaldehyde solution (catalog number BL539A; Biosharp, Hefei, China) to fix mouse tissues. The tissues were then dehydrated using gradient ethanol and embedded in paraffin. All slices (4-μm thickness) were stained with hematoxylin and eosin (catalog number BL700B; Biosharp, Hefei, China) for morphological analysis.

Statistical analysis

Results are presented as means ± SEM. We conducted the statistical analyses using GraphPad Prism software (version 7.0). The statistical differences between two groups were evaluated using two-tailed unpaired Student's t tests. We applied two-way ANOVA tests to assess overall significance and then Bonferroni's multiple comparisons tests. We considered $p < 0.05$ as indicative of statistical significance.

DATA AND CODE AVAILABILITY

All of the study data generated in the article and/or supplemental information during the present study are available from the corresponding author on reasonable request.

ACKNOWLEDGMENTS

This work was supported by the National Natural Science Foundation of China (U1903304, 82160169), the Key Program of Natural Science Foundation of Xinjiang Uygur Autonomous Region (2022D01D16), Major Scientific Research Achievements Cultivation Project of Xinjiang Medical University (XYD2024ZC03), Xinjiang Uygur Autonomous Region Tianshan Innovation Team Program (2024D14011), Training Program of National Science Foundation for Distinguished Young Scholar (xyd2021J004), Xinjiang Uygur Autonomous Region Tianshan Youth Science and Technology Elite Talent Project (2022TSYCCX0031, 2023TSYCQNTJ0027), and State Key Laboratory of Pathogenesis, Prevention, Treatment of Central Asian High Incidence Diseases Fund (SKL-HIDCA2021- XXG3).

AUTHOR CONTRIBUTIONS

X.C. and B.C. designed the study and wrote the original manuscript. X.C., B.C., M.S., X.M., and Y.M. performed experiments. X.C. and B.C. performed data analysis. B.C. reviewed and revised the manuscript. All of the authors read and approved the final manuscript.

DECLARATION OF INTERESTS

The authors declare no competing interests.

SUPPLEMENTAL INFORMATION

Supplemental information can be found online at https://doi.org/10.1016/j.omtm.2024.101390.

REFERENCES

1. Gallino, A., Aboyans, V., Diehm, C., Cosentino, F., Stricker, H., Falk, E., Schouten, O., Lekakis, J., Amann-Vesti, B., Siclari, F., et al. (2014). Non-coronary atherosclerosis. Eur. Heart J. *35*, 1112–1119.
2. Herrington, W., Lacey, B., Sherliker, P., Armitage, J., and Lewington, S. (2016). Epidemiology of Atherosclerosis and the Potential to Reduce the Global Burden of Atherothrombotic Disease. Circ. Res. *118*, 535–546.
3. Pirillo, A., Bonacina, F., Norata, G.D., and Catapano, A.L. (2018). The Interplay of Lipids, Lipoproteins, and Immunity in Atherosclerosis. Curr. Atherosclerosis Rep. *20*, 12.
4. Khalil, M.F., Wagner, W.D., and Goldberg, I.J. (2004). Molecular interactions leading to lipoprotein retention and the initiation of atherosclerosis. Arterioscler. Thromb. Vasc. Biol. *24*, 2211–2218.
5. Wu, M.-Y., Li, C.-J., Hou, M.-F., and Chu, P.-Y. (2017). New Insights into the Role of Inflammation in the Pathogenesis of Atherosclerosis. Int. J. Mol. Sci. *18*, 2034.
6. Abifadel, M., Varret, M., Rabès, J.P., Allard, D., Ouguerram, K., Devillers, M., Cruaud, C., Benjannet, S., Wickham, L., Erlich, D., et al. (2003). Mutations in PCSK9 cause autosomal dominant hypercholesterolemia. Nat. Genet. *34*, 154–156.
7. Benjannet, S., Rhainds, D., Essalmani, R., Mayne, J., Wickham, L., Jin, W., Asselin, M.C., Hamelin, J., Varret, M., Allard, D., et al. (2004). NARC-1/PCSK9 and its natural mutants: zymogen cleavage and effects on the low density lipoprotein (LDL) receptor and LDL cholesterol. J. Biol. Chem. *279*, 48865–48875.
8. Maxwell, K.N., and Breslow, J.L. (2004). Adenoviral-mediated expression of Pcsk9 in mice results in a low-density lipoprotein receptor knockout phenotype. Proc. Natl. Acad. Sci. USA *101*, 7100–7105.
9. Shapiro, M.D., Tavori, H., and Fazio, S. (2018). PCSK9: From Basic Science Discoveries to Clinical Trials. Circ. Res. *122*, 1420–1438.
10. Page, M.M., and Watts, G.F. (2018). PCSK9 in context: A contemporary review of an important biological target for the prevention and treatment of atherosclerotic cardiovascular disease. Diabetes Obes. Metabol. *20*, 270–282.
11. Robinson, J.G., Jayanna, M.B., Brown, A.S., Aspry, K., Orringer, C., Gill, E.A., Goldberg, A., Jones, L.K., Maki, K., Dixon, D.L., et al. (2019). Enhancing the value of PCSK9 monoclonal antibodies by identifying patients most likely to benefit. A consensus statement from the National Lipid Association. J. Clin. Lipidol. *13*, 525–537.
12. Lamb, Y.N. (2021). Inclisiran: First Approval. Drugs *81*, 389–395.
13. Ray, K.K., Raal, F.J., Kallend, D.G., Jaros, M.J., Koenig, W., Leiter, L.A., Landmesser, U., Schwartz, G.G., Lawrence, D., Friedman, A., et al. (2023). Inclisiran and cardiovascular events: a patient-level analysis of phase III trials. Eur. Heart J. *44*, 129–138.
14. Raal, F.J., Kallend, D., Ray, K.K., Turner, T., Koenig, W., Wright, R.S., Wijngaard, P.L.J., Curcio, D., Jaros, M.J., Leiter, L.A., et al. (2020). Inclisiran for the Treatment of Heterozygous Familial Hypercholesterolemia. N. Engl. J. Med. *382*, 1520–1530.
15. Ray, K.K., Troquay, R.P.T., Visseren, F.L.J., Leiter, L.A., Scott Wright, R., Vikarunnessa, S., Talloczy, Z., Zang, X., Maheux, P., Lesogor, A., and Landmesser, U. (2023). Long-term efficacy and safety of inclisiran in patients with high cardiovascular risk and elevated LDL cholesterol (ORION-3): results from the 4-year open-label extension of the ORION-1 trial. Lancet Diabetes Endocrinol. *11*, 109–119.
16. Galactionova, K., Salari, P., Mattli, R., Rachamin, Y., Meier, R., and Schwenkglenks, M. (2022). Cost-Effectiveness, Burden of Disease and Budget Impact of Inclisiran: Dynamic Cohort Modelling of a Real-World Population with Cardiovascular Disease. Pharmacoeconomics *40*, 791–806.
17. Momtazi-Borojeni, A.A., Jaafari, M.R., Afshar, M., Banach, M., and Sahebkar, A. (2021). PCSK9 immunization using nanoliposomes: preventive efficacy against hypercholesterolemia and atherosclerosis. Arch. Med. Sci. *17*, 1365–1377.
18. Sahebkar, A., Momtazi-Borojeni, A.A., and Banach, M. (2021). PCSK9 Vaccine: So Near, yet So Far (Oxford University Press).
19. Lee, R.G., Mazzola, A.M., Braun, M.C., Platt, C., Vafai, S.B., Kathiresan, S., Rohde, E., Bellinger, A.M., and Khera, A.V. (2023). Efficacy and safety of an investigational single-course CRISPR base-editing therapy targeting PCSK9 in nonhuman primate and mouse models. Circulation *147*, 242–253.
20. Nathwani, A.C., Reiss, U.M., Tuddenham, E.G.D., Rosales, C., Chowdary, P., McIntosh, J., Della Peruta, M., Lheriteau, E., Patel, N., Raj, D., et al. (2014). Long-term safety and efficacy of factor IX gene therapy in hemophilia B. N. Engl. J. Med. *371*, 1994–2004.
21. Kattenhorn, L.M., Tipper, C.H., Stoica, L., Geraghty, D.S., Wright, T.L., Clark, K.R., and Wadsworth, S.C. (2016). Adeno-Associated Virus Gene Therapy for Liver Disease. Hum. Gene Ther. *27*, 947–961.
22. Roche-Molina, M., Sanz-Rosa, D., Cruz, F.M., García-Prieto, J., López, S., Abia, R., Muriana, F.J.G., Fuster, V., Ibáñez, B., and Bernal, J.A. (2015). Induction of sustained

hypercholesterolemia by single adeno-associated virus-mediated gene transfer of mutant hPCSK9. Arterioscler. Thromb. Vasc. Biol. *35*, 50–59.

23. Tu, M., Liu, F., Chen, S., Wang, M., and Cheng, A. (2015). Role of capsid proteins in parvoviruses infection. Virol. J. *12*, 114.
24. Zincarelli, C., Soltys, S., Rengo, G., and Rabinowitz, J.E. (2008). Analysis of AAV serotypes 1-9 mediated gene expression and tropism in mice after systemic injection. Mol. Ther. *16*, 1073–1080.
25. Yurtseven, E., Ural, D., Baysal, K., and Tokgözoğlu, L. (2020). An Update on the Role of PCSK9 in Atherosclerosis. J. Atherosclerosis Thromb. *27*, 909–918.
26. van Gestel, M.A., van Erp, S., Sanders, L.E., Brans, M.A.D., Luijendijk, M.C.M., Merkestein, M., Pasterkamp, R.J., and Adan, R.A.H. (2014). shRNA-induced saturation of the microRNA pathway in the rat brain. Gene Ther. *21*, 205–211.
27. Mockenhaupt, S., Grosse, S., Rupp, D., Bartenschlager, R., and Grimm, D. (2015). Alleviation of off-target effects from vector-encoded shRNAs via codelivered RNA decoys. Proc. Natl. Acad. Sci. USA *112*, E4007–E4016.
28. Sun, H., Krauss, R.M., Chang, J.T., and Teng, B.B. (2018). PCSK9 deficiency reduces atherosclerosis, apolipoprotein B secretion, and endothelial dysfunction. J. Lipid Res. *59*, 207–223.
29. Palaschak, B., Herzog, R.W., and Markusic, D.M. (2019). AAV-Mediated Gene Delivery to the Liver: Overview of Current Technologies and Methods. Methods Mol. Biol. *1950*, 333–360.
30. Wang, L., Bell, P., Somanathan, S., Wang, Q., He, Z., Yu, H., McMenamin, D., Goode, T., Calcedo, R., and Wilson, J.M. (2015). Comparative Study of Liver Gene Transfer With AAV Vectors Based on Natural and Engineered AAV Capsids. Mol. Ther. *23*, 1877–1887.
31. Mueller, C., and Flotte, T.R. (2008). Clinical gene therapy using recombinant adeno-associated virus vectors. Gene Ther. *15*, 858–863.
32. Mingozzi, F., and High, K.A. (2011). Therapeutic in vivo gene transfer for genetic disease using AAV: progress and challenges. Nat. Rev. Genet. *12*, 341–355.
33. Mücke, M.M., Fong, S., Foster, G.R., Lillicrap, D., Miesbach, W., and Zeuzem, S. (2024). Adeno-associated viruses for gene therapy - clinical implications and liver-related complications, a guide for hepatologists. J. Hepatol. *80*, 352–361.
34. Frank-Kamenetsky, M., Grefhorst, A., Anderson, N.N., Racie, T.S., Bramlage, B., Akinc, A., Butler, D., Charisse, K., Dorkin, R., Fan, Y., et al. (2008). Therapeutic RNAi targeting PCSK9 acutely lowers plasma cholesterol in rodents and LDL cholesterol in nonhuman primates. Proc. Natl. Acad. Sci. USA *105*, 11915–11920.
35. Denis, M., Marcinkiewicz, J., Zaid, A., Gauthier, D., Poirier, S., Lazure, C., Seidah, N.G., and Prat, A. (2012). Gene inactivation of proprotein convertase subtilisin/kexin type 9 reduces atherosclerosis in mice. Circulation *125*, 894–901.
36. Tang, Z.H., Peng, J., Ren, Z., Yang, J., Li, T.T., Li, T.H., Wang, Z., Wei, D.H., Liu, L.S., Zheng, X.L., and Jiang, Z.S. (2017). New role of PCSK9 in atherosclerotic inflammation promotion involving the TLR4/NF-κB pathway. Atherosclerosis *262*, 113–122.
37. Ason, B., van der Hoorn, J.W.A., Chan, J., Lee, E., Pieterman, E.J., Nguyen, K.K., Di, M., Shetterly, S., Tang, J., Yeh, W.-C., et al. (2014). PCSK9 inhibition fails to alter hepatic LDLR, circulating cholesterol, and atherosclerosis in the absence of ApoE. J. Lipid Res. *55*, 2370–2379.
38. Kounatidis, D., Vallianou, N.G., Poulaki, A., Evangelopoulos, A., Panagopoulos, F., Stratigou, T., Geladari, E., Karampela, I., and Dalamaga, M. (2024). ApoB100 and Atherosclerosis: What's New in the 21st Century? Metabolites *14*, 123.
39. Kothari, V., Ho, T.W.W., Cabodevilla, A.G., He, Y., Kramer, F., Shimizu-Albergine, M., Kanter, J.E., Snell-Bergeon, J., Fisher, E.A., Shao, B., et al. (2024). Imbalance of APOB Lipoproteins and Large HDL in Type 1 Diabetes Drives Atherosclerosis. Circ. Res. *135*, 335–349.
40. Johannesen, C.D.L., Langsted, A., Nordestgaard, B.G., and Mortensen, M.B. (2024). Excess Apolipoprotein B and Cardiovascular Risk in Women and Men. J. Am. Coll. Cardiol. *83*, 2262–2273.
41. Marston, N.A., Giugliano, R.P., Melloni, G.E.M., Park, J.G., Morrill, V., Blazing, M.A., Ference, B., Stein, E., Stroes, E.S., Braunwald, E., et al. (2022). Association of Apolipoprotein B-Containing Lipoproteins and Risk of Myocardial Infarction in Individuals With and Without Atherosclerosis: Distinguishing Between Particle Concentration, Type, and Content. JAMA Cardiol. *7*, 250–256.
42. Tang, Z.H., Li, T., Li, T.H., Zheng, J., Li, T., Liu, L.S., Li, T.T., and Zheng, X.L. (2019). PCSK9: A novel inflammation modulator in atherosclerosis? J. Cell. Physiol. *234*, 2345–2355.
43. Moore, K.J., Sheedy, F.J., and Fisher, E.A. (2013). Macrophages in atherosclerosis: a dynamic balance. Nat. Rev. Immunol. *13*, 709–721.
44. Tavori, H., Giunzioni, I., Predazzi, I.M., Plubell, D., Shivinsky, A., Miles, J., Devay, R.M., Liang, H., Rashid, S., Linton, M.F., and Fazio, S. (2016). Human PCSK9 promotes hepatic lipogenesis and atherosclerosis development via apoE- and LDLR-mediated mechanisms. Cardiovasc. Res. *110*, 268–278.
45. Giunzioni, I., Tavori, H., Covarrubias, R., Major, A.S., Ding, L., Zhang, Y., DeVay, R.M., Hong, L., Fan, D., Predazzi, I.M., et al. (2016). Local effects of human PCSK9 on the atherosclerotic lesion. J. Pathol. *238*, 52–62.
46. Landlinger, C., Pouwer, M.G., Juno, C., van der Hoorn, J.W.A., Pieterman, E.J., Jukema, J.W., Staffler, G., Princen, H.M.G., and Galabova, G. (2017). The AT04A vaccine against proprotein convertase subtilisin/kexin type 9 reduces total cholesterol, vascular inflammation, and atherosclerosis in APOE*3Leiden.CETP mice. Eur. Heart J. *38*, 2499–2507.
47. Kühnast, S., van der Hoorn, J.W.A., Pieterman, E.J., van den Hoek, A.M., Sasiela, W.J., Gusarova, V., Peyman, A., Schäfer, H.-L., Schwahn, U., Jukema, J.W., and Princen, H.M.G. (2014). Alirocumab inhibits atherosclerosis, improves the plaque morphology, and enhances the effects of a statin. J. Lipid Res. *55*, 2103–2112.
48. Steyers, C.M., and Miller, F.J., Jr. (2014). Endothelial dysfunction in chronic inflammatory diseases. Int. J. Mol. Sci. *15*, 11324–11349.
49. Noels, H., Bernhagen, J., and Weber, C. (2009). Macrophage migration inhibitory factor: a noncanonical chemokine important in atherosclerosis. Trends Cardiovasc. Med. *19*, 76–86.
50. Sinitski, D., Kontos, C., Krammer, C., Asare, Y., Kapurniotu, A., and Bernhagen, J. (2019). Macrophage Migration Inhibitory Factor (MIF)-Based Therapeutic Concepts in Atherosclerosis and Inflammation. Thromb. Haemostasis *119*, 553–566.
51. Schmitz, C., Noels, H., El Bounkari, O., Straussfeld, E., Megens, R.T.A., Sternkopf, M., Alampour-Rajabi, S., Krammer, C., Tilstam, P.V., Gerdes, N., et al. (2018). Mif-deficiency favors an atheroprotective autoantibody phenotype in atherosclerosis. Faseb. J. *32*, 4428–4443.
52. Burger-Kentischer, A., Göbel, H., Kleemann, R., Zernecke, A., Bucala, R., Leng, L., Finkelmeier, D., Geiger, G., Schaefer, H.E., Schober, A., et al. (2006). Reduction of the aortic inflammatory response in spontaneous atherosclerosis by blockade of macrophage migration inhibitory factor (MIF). Atherosclerosis *184*, 28–38.
53. Lin, J., Kakkar, V., and Lu, X. (2014). Impact of MCP-1 in atherosclerosis. Curr. Pharmaceut. Des. *20*, 4580–4588.
54. Ference, B.A., Yoo, W., Alesh, I., Mahajan, N., Mirowska, K.K., Mewada, A., Kahn, J., Afonso, L., Williams, K.A., Sr., and Flack, J.M. (2012). Effect of long-term exposure to lower low-density lipoprotein cholesterol beginning early in life on the risk of coronary heart disease: a Mendelian randomization analysis. J. Am. Coll. Cardiol. *60*, 2631–2639.
55. van den Hoek, A.M., van der Hoorn, J.W.A., Maas, A.C., van den Hoogen, R.M., van Nieuwkoop, A., Droog, S., Offerman, E.H., Pieterman, E.J., Havekes, L.M., and Princen, H.M.G. (2014). APOE*3Leiden.CETP transgenic mice as model for pharmaceutical treatment of the metabolic syndrome. Diabetes Obes. Metabol. *16*, 537–544.
56. Chen, H. (2008). Intron splicing-mediated expression of AAV Rep and Cap genes and production of AAV vectors in insect cells. Mol. Ther. *16*, 924–930.
57. Chen, B.D., He, C.H., Chen, X.C., Pan, S., Liu, F., Ma, X., Li, X.M., Gai, M.T., Tao, J., Ma, Y.T., et al. (2015). Targeting transgene to the heart and liver with AAV9 by different promoters. Clin. Exp. Pharmacol. Physiol. *42*, 1108–1117.
58. Andrés-Manzano, M.J., Andres, V., and Dorado, B. (2015). Oil Red O and Hematoxylin and Eosin Staining for Quantification of Atherosclerosis Burden in Mouse Aorta and Aortic Root. Methods in mouse atherosclerosis *1339*, 85–99.